Research, Society and Development, v. 9, n. 3, e42932022, 2020
(CC BY 4.0) | ISSN 2525-3409 | DOI: http://dx.doi.org/10.33448/rsd-v9i3.2022

Predição do ponto de impacto para rastreamento de foguetes usando os filtros α-β, Kalman padrão, Kalman estendido e Kalman sem cheiro: uma análise comparativa

Rocket tracking impact point prediction using α-β, standard Kalman, extended, Kalman, and unscented Kalman filters: a comparative analysis

Predicción del punto de impacto del seguimiento de cohetes utilizando filtros α-β, Kalman estándar, Kalman extendido y Kalman sin perfume: un análisis comparativo

Recebido: 06/11/2019 | Revisado: 07/11/2019 | Aceito: 12/12/2019 | Publicado: 20/12/2019

José Alano Peres de Abreu
ORCID: https://orcid.org/0000-0001-5614-3754
Federal University of Pará, Brazil
E-mail: alanoabreu@gmail.com
Roberto Célio Limão de Oliveira
ORCID: https://orcid.org/0000-0002-6640-3182
Federal University of Pará, Brazil
E-mail: limao@ufpa.br
João Viana da Fonseca Neto
ORCID: https://orcid.org/0000-0003-4606-7510
Federal University of Maranhão, Brazil
E-mail: jviana@dee.ufma.br

Resumo

Informações precisas sobre o ponto de impacto (PI) de um foguete suborbital na superfície da Terra durante um lançamento são requisitos importantes para operações de segurança dos sítos de lançamento. Quatro estimadores diferentes, como filtro α-β, filtro Kalman padrão (FKP), filtro Kalman estendido (FKE) e filtro Kalman sem cheiro (FKU), são considerados para o problema de rastreamento suborbital de foguetes, cujos dados são usados especificamente para melhorar a precisão da predição do PI (PPI) desses veículos. Este artigo apresenta uma análise comparativa entre os resultados dos estimadores. Os dados de voo de foguetes são analisados no sentido de demonstrar as vantagens e desvantagens dos estimadores e determinar as limitações inerentes à previsão dos efeitos aerodinâmicos encontrados em determinadas situações de voo. Discutimos o modelo matemático apropriado de um filtro capaz de executar o algoritmo em tempo real para as estimativas da posição e

velocidade do alvo. Este trabalho utiliza dados reais de um sensor de radar para avaliar os algoritmos de rastreamento. Inserimos o resultado do filtro no modelo matemático desenvolvido para prever o PI do foguete na superfície da Terra. O principal objetivo deste estudo é avaliar o desempenho de quatro estimadores diferentes, quando aplicados especificamente na melhoria da PPI de foguetes suborbitais. É demonstrado que o FKU supera todos os outros algoritmos de rastreamento em termos de precisão e robustez da estimativa do PI.

Palavras-chave: Estimativa de estado; Algoritmo de rastreamento; Processamento digital de sinais; Previsão de pontos de impacto.

Abstract

Accurate information about the impact point (IP) of a suborbital rocket on Earth’s surface during a launch is an important requirement for range safety operations. Four different estimators, i.e., the α-β filter, standard Kalman filter (SKF), extended Kalman filter (EKF), and unscented Kalman filter (UKF), are considered for the suborbital rocket tracking problem, whose data are used specifically for improving the accuracy of the IP prediction (IPP) of these vehicles. This paper presents a comparative analysis between the results of the estimators. Rocket flight data are discussed to demonstrate the advantages and disadvantages of the estimators and to determine the inherent limitations in predicting the aerodynamic effects found in certain flight situations. We discuss the appropriate mathematical model of a filter capable of running the real-time algorithm for the estimation of target position and velocity. This work uses actual data from a radar sensor to evaluate the tracking algorithms. We insert the filter result into the mathematical model developed to predict the rocket IP on Earth's surface. The main goal of this study is to evaluate the performance of four different estimators when specifically applied for the improvement of the IPP of suborbital rockets. It is demonstrated that the UKF outperforms all other tracking algorithms in terms of the accuracy and robustness of IP estimation.

Keywords: State estimation; Tracking algorithm; Digital signal processing; Impact point prediction.

Resumen

La información precisa sobre el punto de impacto (PI) de un cohete suborbital en la superficie de la Tierra durante un lanzamiento es un requisito importante para las operaciones de seguridad del sitio de lanzamiento. Se consideran cuatro estimadores diferentes, como el filtro

α-β, el filtro Kalman estándar (FKP), el filtro Kalman extendido (FKE) y el filtro Kalman inodoro (FKU) para el problema de seguimiento de cohetes suborbitales, cuyos datos se utilizan específicamente para mejorar la precisión de predicción de PI (PPI) de estos vehículos. Este artículo presenta un análisis comparativo entre los resultados de los estimadores. Los datos del vuelo del cohete se analizan para demostrar las ventajas y desventajas de los estimadores y para determinar las limitaciones inherentes a la predicción de los efectos aerodinámicos encontrados en ciertas situaciones de vuelo. Discutimos el modelo matemático apropiado de un filtro capaz de ejecutar el algoritmo en tiempo real para estimar la posición y la velocidad del objetivo. Este trabajo utiliza datos reales de un sensor de radar para evaluar los algoritmos de seguimiento. Insertamos el resultado del filtro en el modelo matemático desarrollado para predecir el PI del cohete en la superficie de la Tierra. El objetivo principal de este estudio es evaluar el rendimiento de cuatro estimadores diferentes, cuando se aplica específicamente para mejorar el PPI del cohete suborbital. Se muestra que FKU supera a todos los demás algoritmos de seguimiento en términos de precisión y solidez de la estimación de PI.

Palabras clave: Estimación del estado; Algoritmo de seguimiento; Procesamiento de señales digitales; Predicción del punto de impacto.

1. Introduction

Numerous suborbital rockets are launched with the goal of performing scientific and technological experiments. These rockets carry scientific payloads into space for conducting research in the microgravity environment. Consequently, these payloads are recovered as they fall on Earth's surface. The rescue teams that participate in the recovery of these payloads require information on latitude, longitude, and target impact time (Markgraf, Montenbruck, Turner & Viertotak, 2003). There are several methods of locating and rescuing the payload of a space vehicle or a high dynamic vehicle (Montenbruck, Markgraf, Jung, Bull & Engler, 2002). In this work, we utilize a rocket tracking system with a radar sensor. The main advantage of the radar sensor in sounding rocket tracking is that it provides superior penetration capability in any weather condition.

The main goal of this study is to evaluate the performance of four different position and velocity estimators through comparative analysis and to determine their advantages and disadvantages when specifically applied for the improvement of the IPP of suborbital rockets. The α-β filter, SKF, EKF, and UKF estimators are the core of the indirect measurement

system, and they are based on the rocket state-space model. IPP depends on the accuracy and stability of a filter, whose results are the estimated position and velocity of a target.

The problem of the state estimation of the position and velocity of space vehicles has been the object of study of researchers for theoretical, practical, and economical reasons (Ramachandra, 2018; Simon, 2006). These studies aim to develop and apply more robust algorithms for real-world problems. Considering such requirements, the α-β filter (Kosuge, Ito, Okada & Mano, 2002; Ng, Yeong, Su & Wong, 2012; Tenne & Singh, 2002; Yadav, Naik, Ananthasayanam, Gaur & Singh, 2012) and SKF (Abreu, Neto & Oliveira, 2011; Chui & Chen, 2008; Kalman, 1960; Welch & Bishop, 2006) were the most widely used algorithms. However, the α-β filter and SKF can be optimally applied only to problems that can be represented by linear systems. The α-β filter is widely used for the tracking of sounding rockets. Currently, it is employed at Brazilian, Swedish, and Norwegian launch sites for the filtering of radar signals in tracking rockets (Garcia, Yamanaka, Barbosa, Bizarria, Jung & Scheuerpflug, 2011). Despite its wide use, the α-β filter has the following limitations: It is suboptimal, and constant gains are computed a priori and provided as input to the tracking algorithm (Yadav, Naik, Ananthasayanam, Gaur & Singh, 2012). Owing to the lack of recursion, this filter can cause aberrant results in the cases of abnormality in flight (Abreu, Neto & Oliveira, 2011). Other techniques have been studied and developed to overcome these limitations; for example, the EKF (Einicke & White, 1999; Farina, Ristic & Benvenuti, 2002) and UKF (Biswas, Southwell & Dempster, 2018; Garcia, Pardal, Kuga & Zanardi, 2019; Julier & Uhlmann, 2004; Scardua & da Cruz, 2016; Wan & Van Der Merwe, 2000).

The EKF is the most commonly used nonlinear filtering algorithm for position and velocity estimation in real time. However, when the filter is subjected to poor conditions, the linearization of a system may not be efficient, and this may lead to low accuracy estimation and even filter divergence. The UKF algorithm was developed to eliminate the linearization required by the EKF (Julier & Uhlmann, 2004). The main advantages of the UKF over EKF are that the expected error of the UKF is smaller compared to the EKF and the UKF does not require the derivation of Jacobian matrices. The UKF exhibited more accurate and robust performance compared to the EKF under inaccurate initial conditions (Garcia, Kuga & Zanardi, 2016). The UKF uses a set of points that are selected deterministically, which are referred to as ‘‘sigma points,” to capture a probability distribution and generalizes to a nonlinear system without the burdensome analytic derivation required in the EKF (Julier & Uhlmann, 2004).

This work aims to analyze the behavior of the α-β, SKF, EKF, and UKF estimators when applied to actual position data obtained from rocket tracking to improve IPP. At present and to the best of our knowledge, this is the first time that the comparative analysis among these four estimators has been applied to the problem of position and velocity estimation to predict the IP using actual data. Analyzing the behavior of algorithms when they are applied to actual data poses practical difficulties such as the tuning and learning of filters.

The contribution of this paper is the performance analysis of the UKF nonlinear estimator applied to the problem of position and velocity estimation to improve IPP for actual data measured by a radar sensor. The data refer to the tracking of suborbital rockets launched at the Alcântara Launch Center.

The rest of this paper is structured as follows: Section 2 describes the methods involved in the rocket tracking process and real-time IPP modeling. Section 3 describes the modeling of the α-β, SKF, EKF, and UKF estimators. Section 4 describes the results obtained in the study through the comparative analysis of the four different estimators and IPP model. Section 5 summarizes our work.

2. Target tracking impact point

2.1. Rocket tracking process

The structure established in this work for the comparative analysis of the four tracking algorithms used for rocket tracking IPP is shown in Fig. 1.

Figure.1: Steps of estimation and IPP of rocket on Earth's surface.

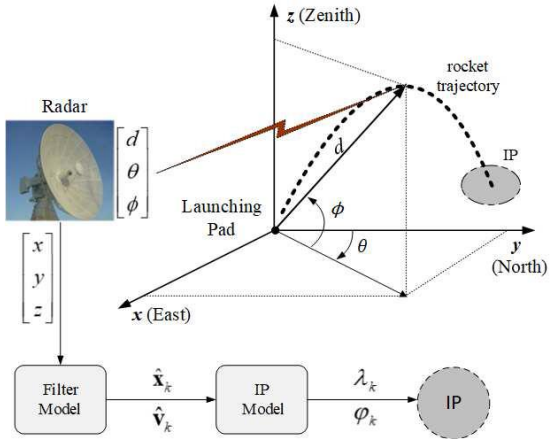

Source: Authors.

The filtering process is used to estimate the position ($\hat{x}_k$), and velocity ($\hat{v}_k$), of the rocket during tracking. After filtering, the estimated data are sent to the input of the IPP

calculation algorithm, which generates and plots the results in latitude (λ_k), longitude (φ_k), and impact-time (t_k) coordinates.

Initially, raw position data are measured by the radar sensor in spherical coordinates, $[d, \quad \theta, \quad \phi]^T$, as follows:

$$d = \sqrt{x^2 + y^2 + z^2} \ , \tag{1}$$

$$\theta = \arctan\left(\frac{y}{x}\right) \ , \tag{2}$$

$$\phi = \arctan\left(\frac{\sqrt{x^2 + y^2}}{z}\right) \tag{3}$$

These coordinates are transformed into Cartesian coordinates $[\mathrm{x}, \quad \mathrm{y}, \quad z]^T$, given by

$$x = d\cos(\phi)\sin(\theta) \ , \tag{4}$$

$$y = d\cos(\phi)\cos(\theta) \tag{5}$$

$$z = d\sin\phi \tag{6}$$

Consequently, signals are filtered and presented as the estimated position vector $\hat{x}_k = [\hat{x}, \quad \hat{y}, \quad \hat{z}]^T$, and estimated velocity vector $\hat{v}_k = [\hat{v}_x, \quad \hat{v}_y, \quad \hat{v}_z]^T$. The estimated position and velocity signals available at the output of the tracking algorithm are used to calculate the IP on Earth's surface (Markgraf, Montenbruck, Turner & Viertotak, 2003; Jung & Hwang, 2013).

2.2. Impact point problem

This section presents the real-time computation performed using the rocket's IPP model. The trajectory of the rocket is ballistic owing to a stop in propulsion. The input data of the IPP algorithm are the Cartesian coordinates of the position $(\hat{x}, \quad \hat{y}, \quad \hat{z})$ and the rocket velocity $(\hat{v}_x \quad \hat{v}_y \quad \hat{v}_z)$ within terrestrial geographical reference, as shown in Fig. 1. The output data of this module are the geocentric coordinates, latitude (λ_k), and longitude (φ_k) of the IP and the flight time (t_k) until impact. The complete IPP process consists of two functional blocks in a broad sense, one for the filtering of radar signals and the other for predicting the IP position.

The problem of IPP involves the use of digital filters to estimate rocket position and velocity to calculate latitude, longitude, and impact time parameters. The solution to this problem considers the development of system dynamic models that are used by a filter and the computation of the IP (Wang & Chang, 2013). Thus, the IPP problem is characterized as an estimation problem during flight from the point of view of the laws of classical mechanics, and it considers the position signals captured by the radar sensor as input (Jung & Hwang, 2013).

The problem is formulated using stochastic filtering techniques. The IP reflects the noise level of a filtered signal and the reaction time of a filter in the transitions between propelled (powered ascent) and ballistic phases. The quality of the prediction and evolution of the IP depend on the accuracy, stability, noise level, and convergence velocity of a filter. The constraints in using the technique for filtering multistage rocket tracking data and the prediction of the evolution of the IP obey filter performance limits (Bozic, 1983).

One of the main purposes of flight safety during rocket tracking is the ability to track the trajectory of the rocket and adjust the location of the IP with respect to Earth's surface considering the propelled phase (powered ascent) at every moment. Therefore, gains should be adjusted according to time.

2.3. Impact point model

The model for IPP is discussed in this section. Through the basic equations and the behavior of an IP curve, we can observe the noise level of a filtered signal and the response time of a filter for the following situations: between the stages of burning end and the start of the next burning; filtering in the ballistic phase; between the moments of the loss and reacquisition of a target.

The model considers the following assumptions for determining the IP, as shown in Fig. 2. The trajectory of the rocket is purely ballistic, i.e., elliptical according to Kepler's laws; The movement is calculated in relation to the center of gravity of the vehicle in flight; The terrestrial relief and the friction in the atmosphere are not considered; Earth is considered spherical; The IP is calculated at zero altitude.

Figure.2: Estimated vectors of position and velocity on an elliptical trajectory of IPP.

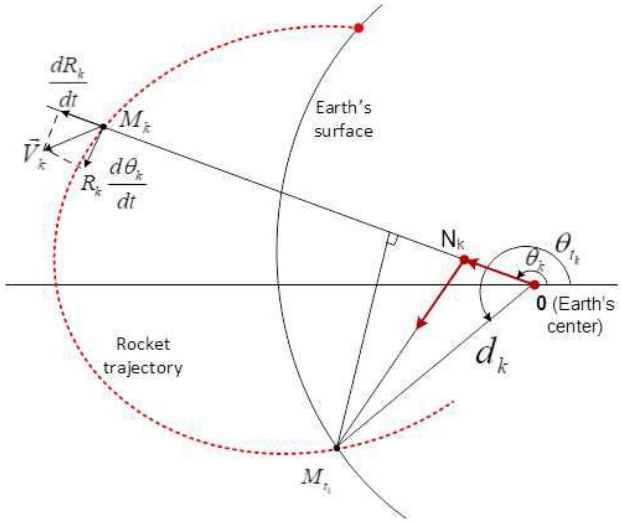

Source: Authors.

2.4. Latitude and longitude calculation

Using the reference system that considers the center of Earth as the origin, the z axis is Earth's rotation axis, the x axis is given by the intersection of the plane defined by the Greenwich meridian with the plane of the equator, and the y axis is normal to the plane defined by the x and z axes. Once the position $O\vec{M}_k = \hat{x}_k$, and velocity $\hat{v}_k$, vectors are known and obtained from the filtering process, which is described in Section 3, the computation of the position vector of the IP, $O\vec{M}_{t_k}$, consists of determining coefficients F_k and G_k, as presented in Fig. 2.

$$\overrightarrow{OM_{t_k}} = \overrightarrow{ON_k} + \overrightarrow{N_k M_{t_k}} . \tag{7}$$

Equation (7) can also be written as

$$\overrightarrow{OM_{t_k}} = F_k \hat{x}_k + G_k \hat{v}_k , \tag{8}$$

Where $\hat{x}_k$ and $\hat{v}_k$ are known. This is sufficient for determining F_k and G_k, where F_k is the projection of equation (8) on vector $\hat{x}_k$ and G_k is the projection of equation (8) on perpendicular vector $\hat{x}_k$. F_k and G_k are given by

$$F_k = \frac{\cos(\mathrm{E}_{t_k} - \mathrm{E}_k) - e\cos(\mathrm{E}_k)}{1 - e\cos(\mathrm{E}_k)} \tag{9}$$

and

$$G_k = \frac{a^{3/2}}{\mu}[\sin(\mathrm{E}_{t_k} - \mathrm{E}_k) - e(\sin(\mathrm{E}_{t_k} - \mathrm{E}_k)], \tag{10}$$

where a is the semi-major axis of the ellipse, μ is the standard gravitational parameter, e is the eccentricity of the ellipse, E_t is the eccentric anomaly at time *t*, and E_{t_k} is the eccentric anomaly at the time of impact.

In sequence, the successive projections of equation (8) are calculated over the line containing the impact vector $\hat{x}_k$, and its perpendicular. In Galilean geocentric reference, the IP vector is given by

$$\overrightarrow{OM_{t_k}} = F_k \hat{x}_k + G_k \hat{v}_k = \vec{d}_{t_k} \tag{11}$$

where x_k, y_k, and z_k are the IP coordinates, as shown in Fig. 3. Therefore, the latitude and longitude of this IP are given by

$$\lambda_k = \arctan\left(\frac{z_k}{\sqrt{x_k^2 + y_k^2}}\right) \tag{12}$$

and

$$\varphi_k = \arctan\left(\frac{y_k}{x_k}\right) \tag{13}$$

Figure.3: Projection of the impact point vector $\overrightarrow{OM}_{t_k}$, on x_k, y_k, and z_k coordinates.

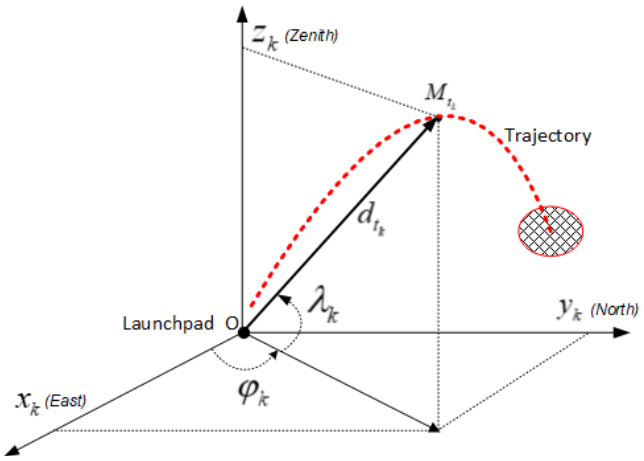

Source: Authors.

3. Experimental procedure (Analyzed estimators)

This section presents the four different tracking algorithms. We describe the $\alpha-\beta$ filter and SKF in the linear representation and the EKF and UKF in the nonlinear representation (AminiOmam, Torkamani-Azar & Ghorashi, 2017). The data obtained through

these estimators are used as the input to the IPP algorithm. IPP depends on the accuracy and stability of the filter that contributes to the filtered signals of the estimated position and velocity.

3.1. $\alpha-\beta$ Filter

The $\alpha-\beta$ filter is a constant gain estimator used specifically in tracking systems when position measurements are available in Cartesian coordinates and when the state vector consists of position and velocity. The $\alpha-\beta$ filter estimates the next step of the states of a system according to the typical equations of kinematics and corrects these estimations through the multiplication of positions estimation residuals with constant gains. The $\alpha-\beta$ filter predicts the position and velocity that describe the dynamics of rocket flight (Kosuge, Ito, Okada & Mano, 2002; Ng, Yeong, Su & Wong, 2012; Tenne & Singh, 2002; Wu, Chang & Chu, 2011).

To establish a radar signal processing scheme (Greco, Abramovich, Ovarlez & Yang, 2015), it is necessary to introduce the predicted position, predicted velocity, estimated position, and estimated velocity equations, which are respectively given by

$$x_p(\mathrm{k+1}) = x_s(\mathrm{k}) + \mathrm{T}\,v_s(k)\,, \tag{14}$$

$$v_p(\mathrm{k+1}) = v_s(\mathrm{k})\,, \tag{15}$$

$$\hat{x}_{s_k} = x_{p_k} + \alpha[x_k - x_{p_k}], \alpha > 0\,, \tag{16}$$

$$\hat{v}_{s_k} = v_{p_k} + (\beta/T)[x_k - x_{p_k}], \beta > 0\,. \tag{17}$$

3.2. Standard Kalman filter

The SKF is essentially a set of mathematical equations that implement an optimal predictor-corrector type estimator to minimize estimated error covariance when certain conditions are met (Welch & Bishop, 2006). The SKF describes a recursive solution for data estimation, and it is applied optimally only in problems that can be represented by a discrete linear system. Owing to efficient recursive performance and advances in computing, the SKF has a wide range of applications, particularly in space, such as rocket trajectory analysis (Chui & Chen, 2008; Kalman, 1960; Bozic, 1983).

The state-space model implemented from the process and measurement is given by transition and observation equations.

$$x_{k+1} = Ax_k + w_k\,, \tag{18}$$

$$y_k = Cx_k + \eta_k\,. \tag{19}$$

The SKF equations are divided into two groups, i.e., ``time update" and ``measurement update" equations. The time update (prediction) equations are as follows:

$$\hat{x}_{k/k-1} = A\hat{x}_{k-1/k-1}\,, \tag{20}$$

$$P_{k/k-1} = AP_{k-1/k-1}A^T + Q_k\,, \tag{21}$$

$$\hat{y}_k = C\hat{x}_{k/k-1}\,. \tag{22}$$

The measurement update (correction) equations are as follows:

$$K_k = P_{k/k-1}C^T[\mathrm{C}\,P_{k/k-1}C^T + \mathrm{R}_k]^{-1}\,, \tag{23}$$

$$\hat{x}_{k/k} = \hat{x}_{k/k-1} + K_k[\mathrm{y}_k - \hat{\mathrm{y}}_k]\,, \tag{24}$$

$$P_{k/k} = P_{k/k-1} - K_k CP_{k/k-1}\,. \tag{25}$$

3.3. Extended Kalman filter

The EKF is widely used for the state estimation of nonlinear systems. One of the possible approaches is to linearize the system under investigation around its current state and force the filter to use the linearized version of the system as a model. Specifically, in this work, the EKF describes a recursive solution for the state estimation problems of a discrete nonlinear system.

Given an initial value, one can predict and adjust the parameters of a system model through each new measurement to yield the estimated error on each update. Owing to recursive performance and progress in computing, the EKF has a wide range of applications, particularly in space, such as rocket trajectory analysis (Einicke & White, 1999).

The state-space model implemented from the process and measurement is given by transition and observation equations.

$$x_{k+1} = Ax_k + w_k\,, \tag{26}$$

$$y_k = h(x_k) + \eta_k\,, \tag{27}$$

Where x_k is the tracking state vector, which indicates position $\left[x, \quad y, \quad z\right]^T$ and velocity $\left[v_x, \quad v_y, \quad v_z\right]^T$, and y_k is the vector of spherical coordinate measurements. $h(.)$ is the Cartesian-to-spherical coordinate transformation. Vector y_k represents the position measurement by the radar sensor at coordinates $\left(d, \quad \theta, \quad \phi\right)$. The measurement of the spherical coordinates of the position of a target related to the state of the Cartesian coordinates is given by

$$y_k = \begin{bmatrix} d \\ \theta \\ \phi \end{bmatrix} = \begin{bmatrix} \sqrt{x_k^2 + y_k^2 + z_k^2} \\ \tan^{-1}\left(\frac{y_k}{x_k}\right) \\ \tan^{-1}\left(\frac{\sqrt{x_k + y_k}}{z_k}\right) \end{bmatrix} + \begin{bmatrix} \eta_{x_k} \\ \eta_{y_k} \\ \eta_{z_k} \end{bmatrix} \tag{28}$$

The EKF equations are divided into two groups, i.e., “time update" and “measurement update" equations.

The time update equations (prediction) are given by

$$\hat{x}_{k/k-1} = A\hat{x}_{k-1/k-1}, \tag{29}$$

$$P_{k/k-1} = AP_{k-1/k-1}A^T + Q_k, \tag{30}$$

$$\hat{y}_k = h(\hat{x}_{k/k-1}). \tag{31}$$

The measurement update equations (correction) are given by

$$K_k = P_{k/k-1}\,\mathrm{H}_k^T[\mathrm{H}_k\,P_{k/k-1}H_k^T + \mathrm{R}_k]^{-1}, \tag{32}$$

$$\hat{x}_{k/k} = \hat{x}_{k/k-1} + K_k[\mathrm{y}_k - \hat{\mathrm{y}}_k], \tag{33}$$

$$P_{k/k} = P_{k/k-1} - K_k H_k P_{k/k-1}, \tag{34}$$

where

$$H_k = \left[\frac{\partial h(x_k)}{\partial x_k}\right]_{\hat{x}_{k/k-1}} = \begin{bmatrix} \frac{\hat{x}_{k/k-1}}{h_1} & 0 & \frac{\hat{y}_{k/k-1}}{h_1} & 0 & \frac{\hat{z}_{k/k-1}}{h_1} & 0 \\ \frac{\hat{y}_{k/k-1}}{h_2} & 0 & \frac{\hat{x}_{k/k-1}}{h_2} & 0 & 0 & 0 \\ \frac{2\hat{x}_{k/k-1}\hat{z}_{k/k-1}}{h_3} & 0 & \frac{2\hat{y}_{k/k-1}\hat{z}_{k/k-1}}{h_3} & 0 & \frac{\hat{x}_{k/k-1}^2 + \hat{y}_{k/k-1}^2}{h_3} & 0 \end{bmatrix} \tag{35}$$

is valid only when denominators h_1, h_2, and, h_3 of equation (35) are given by: $h_1 = \sqrt{\hat{x}^2_{k/k-1} + \hat{y}^2_{k/k-1} + \hat{z}^2_{k/k-1}}$; $h_2 = \hat{x}^2_{k/k-1} + \hat{y}^2_{k/k-1}$; $h_3 = \hat{x}^2_{k/k-1} + \hat{y}^2_{k/k-1} + \hat{z}^2_{k/k-1}$.

The deployment of this algorithm is based on an optimality criterion, such as the minimum mean square error, to estimate the state vector.

3.4. Unscented Kalman filter

A method of reducing the linearization errors in the EKF is to consider the UKF. The UKF propagates the Gaussian random variables that represent the state through dynamic systems using a deterministic sampling approach. The state distribution is represented using a minimal set of carefully selected sample points. These sample points completely capture the true mean and covariance of the state, and when propagated through the true nonlinear system, capture the posterior mean and covariance accurately to the second order for any nonlinearity (Biswas, Southwell & Dempster, 2018; Garcia, Pardal, Kuga & Zanardi, 2019; Julier & Uhlmann, 2004; Wan & Van Der Merwe, 2000).

The UKF is an algorithm capable of performing state estimation in systems with nonlinearity without linearizing the nonlinear functions present in the model. This estimation becomes possible owing to a transformation technique that generates a set of vectors that, when undergoing a nonlinear transformation, remain with the same mean and covariance as those of the random variables before the transformation. This technique is known as unscented transformation.

This filter has an advantage when compared to the EKF because the unscented transformation describes the nonlinear system better compared to linearization. Hence, this filter converges to the right solution more rapidly. Another advantage of the UKF is that the calculation of the first-order Jacobian, which can be a challenging task, is not necessary. The UKF is typically more accurate than the EKF because it is able to capture a higher order of nonlinearities (Gadsden, Dunne, Habibi & Kirubarajan, 2009). However, similar to the EKF, the UKF may become unstable and results may be biased.

The UKF is a sigma point Kalman filter that derives the location of sigma points and their corresponding weights according to the following rationale: The sigma points should be selected so that they capture the most important statistical properties of the prior random variable (Van Der Merwe, 2004; Wan, 2006).

The state-space model implemented from the process and measurement is given by transition and observation equations.

$$x_k = f(x_{k-1}) + w_{k-1}, \tag{36}$$

$$y_k = h(x_k) + \eta_k, \tag{37}$$

where x_k is the state vector and y_k is the observation vector. Process noise and observation noise are represented by w_k and η_k, respectively, and they are uncorrelated and Gaussian random processes.

The set of equations that define the UKF algorithm are described below.

Time update equations (Prediction):

a) Generation of sigma points, $\chi_{k-1}^{(i)}$ $(i = 0,1,\ldots,2\,\mathrm{n})$, and the associated weights:

$$\begin{aligned} &\chi_{k-1}^{(0)} = \hat{x}_{k-1}, i = 0 \\ &\chi_{k-1}^{(i)} = \hat{x}_{k-1} + (\sqrt{(n+\kappa)\,\mathrm{P}_{k-1}})_i, \quad i = 1,\ldots,n \\ &\chi_{k-1}^{(i)} = \hat{x}_{k-1} - (\sqrt{(n+\kappa)\,\mathrm{P}_{k-1}})_{i-n}, i = 1, n+1,\ldots,2n \end{aligned} \tag{38}$$

where $\kappa \in \Re$ is a scaling parameter, n is the dimension of the state, $(\sqrt{(n+\kappa)\,\mathrm{P}_{k-1}})$ is the ith row or column of the matrix square root of $(n+\kappa)\,\mathrm{P}_{k-1}$, and W_i is the weight that is associated with the ith point.

b) Propagation of sigma points:

The propagation of each vector $\chi^{(i)}$, through nonlinear functions, f, is given by

$$\chi_{k/k-1}^{(i)} = f(\chi_{k-1}^{(i)}) \quad (i = 0,1,\ldots,2n)$$

c) Estimation of the propagated state and covariance matrix or instant k:

The predicted mean is calculated as

$$\hat{x}_{k/k-1} = \frac{\kappa}{n+\kappa}\chi_{k/k-1}^{(0)} + \sum_{i=1}^{2n}\frac{1}{2(n+\kappa)}\chi_{k/k-1}^{(i)}$$

The predicted covariance is calculated as

$$P_{k/k-1} = \frac{\kappa}{n+\kappa}\left[\chi_{k/k-1}^{(0)} - \hat{x}_{k/k-1}\right]\left[\chi_{k/k-1}^{(0)} - \hat{x}_{k/k-1}\right]^T + \sum_{i=1}^{2n}\frac{1}{2(n+\kappa)}\left[\chi_{k/k-1}^{(0)} - \hat{x}_{k/k-1}\right]\left[\chi_{k/k-1}^{(0)} - \hat{x}_{k/k-1}\right]^T + Q_{k-1} \tag{39}$$

Measurement update equations (Correction)

Similar to time update, a set of $2n+1$ sigma points $\left(\chi_{k-1}^{(i)},\ i = 0,1,\ldots,2n\right)$ are derived from the updated state and covariance matrices, where n is the dimension of the state. The sigma points are propagated through observation function h as follows:

a) Evaluation of sigma points, $\left(\chi_k^{(i)},\ i = 0,\ldots,2n\right)$:

$$\begin{aligned}\chi_k^{(0)} &= \hat{x}_{k/k-1} \\ \chi_k^{(i)} &= \hat{x}_{k/k-1} + (\sqrt{(n-\kappa)\,\mathrm{P}_{k/k-1}})_i, \quad i = 1,\ldots,n \\ \chi_k^{(i)} &= \hat{x}_{k/k-1} - (\sqrt{(n+\kappa)\,\mathrm{P}_{k/k-1}})_{i-n}, i = 1, n+1,\ldots,2n\end{aligned} \tag{40}$$

b) Propagation of sigma points through the measurement model:

$$y_k^{(i)} = h(\chi_k^{(i)}), \quad i = 0,\ldots,2n \tag{41}$$

c) Estimation of the predicted measurement, innovation covariance matrix, and cross-covariance matrix:

$$\hat{y}_k = \frac{\kappa}{n+\kappa} y_k^{(0)} - \sum_{i=1}^{2n} \frac{1}{2(n+\kappa)} y_k^{(i)} \tag{42}$$

$$P_{y_k y_k} = \frac{\kappa}{n+\kappa}\left[y_k^{(0)} - \hat{y}_k\right]\left[y_k^{(0)} - \hat{y}_k\right]^T + \sum_{i=1}^{2n} \frac{1}{2(n+\kappa)}\left[y_k^{(0)} - \hat{y}_k\right]\left[y_k^{(0)} - \hat{y}_k\right]^T + R_k \tag{43}$$

$$P_{x_k y_k} = \frac{\kappa}{n+\kappa}\left[\chi_k^{(0)} - \hat{x}_{k/k-1}\right]\left[y_k^{(0)} - \hat{y}_k\right]^T + \sum_{i=1}^{2n} \frac{1}{2(n+\kappa)}\left[\chi_k^{(i)} - x_{k/k-1}\right]\left[y_k^{(i)} - \hat{y}_k\right]^T \tag{44}$$

d) Estimation of the UKF gain, update state, and covariance matrix:

$$K_k = P_{x_k y_k} P_{y_k y_k}^{-1}, \tag{45}$$

$$\hat{x}_{k/k} = \hat{x}_{k/k-1} + K_k(\mathrm{y}_k - \hat{\mathrm{y}}_{k/k-1}), \tag{46}$$

$$P_{k/k} = P_{k/k-1} - K_k P_{y_k y_k} K_k^T \tag{47}$$

4. Results and comparative analysis

In this section, we present the comparative results of the performance of the α-β, SKF, EKF, and UKF estimators in the tracking of two suborbital rockets and consequently the effect of these results on the IPP problem. The actual data measured by the radar sensor during rocket tracking are considered. Two databases are used, one single-stage rocket (*1-Stg Rocket*) and one two-stage rocket (*2-Stg Rocket*) with a parachute (Garcia, Yamanaka, Barbosa, Bizarria, Jung & Scheuerpflug, 2011). The algorithms are initialized by selecting the parameters that best adjust the behavior of the estimators with respect to their convergence. The parameters selected to initialize the algorithms are α=0.34, β=0.07, Q_0=Diag(0.05 0.05 0.05 0.05 0.05 0.05), R_0=Diag(10 10 10), $\hat{x}_0 = [0 \quad 0 \quad 0 \quad 0 \quad 0 \quad 0]^T$, T=0.05 s, P_0=10 x I_{6x6}, λ_0=-2.3155 (º), and φ_0=-44.29 (º).

Tables 1 and 2 show the mean squared error (MSE), which is also referred to as the estimated error covariance, and the root MSE (RMSE), which is also referred to as the

estimated error standard deviation, of the α-β, SKF, EKF, and UKF estimators. Tables 1 and 2 show that the results obtained by the nonlinear algorithms (EKF and UKF) are better compared to the linear algorithms (α-β and SKF) and that the UKF shows the lowest mean and estimated error standard deviation on the three axes. Figures 4 and 5 show the estimated velocity on the three axes for the α-β, SKF, EKF, and UKF estimators.

Table 1: Mean squared error ± standard deviation of the residuals on the X, Y, Z axes (*1-Stg Rocket*).

	X-Axis (m)	Y-Axis (m)	Z-Axis (m)
α-β	3861 ± 61.91	2899 ± 54.66	5863 ± 81.69
SKF	4730 ± 76.84	3450 ± 66.36	6489 ± 96.41
EKF	41.31 ± 6.42	0.64 ± 1.02	0.9684 ± 0.98
UKF	29.93 ± 5.47	0.001 ± 0.03	0.0002 ± 0.05

Source: Research data by Authors.

Table 2: Mean squared error ± standard deviation of the residuals on the X, Y, Z axes (*2-Stg Rocket*).

	X-Axis (m)	Y-Axis (m)	Z-Axis (m)
α-β	163.37 ± 12.78	49.540 ± 07.03	1574.90 ± 39.60
SKF	752.85 ± 27.43	285.70 ± 16.90	1486.10 ± 121.90
EKF	186.06 ± 13.64	0.0060 ± 0.07	0.05000 ± 0.23
UKF	32.83 ± 5.73	0.00017 ± 0.0013	0.00030 ± 0.006

Source: Research data by Authors.

Figure.4: (1-Stg Rocket) Velocity estimated by α-β, SKF, EKF, and UKF

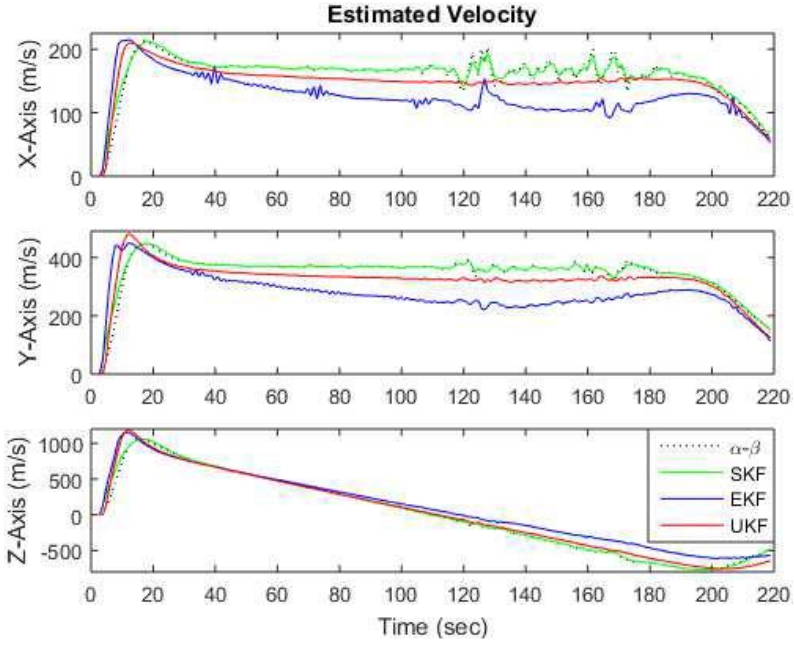

Source: MATLAB Implementation by Authors.

Figure.5: (2-Stg Rocket) Velocity estimated by α-β, SKF, EKF, and UKF

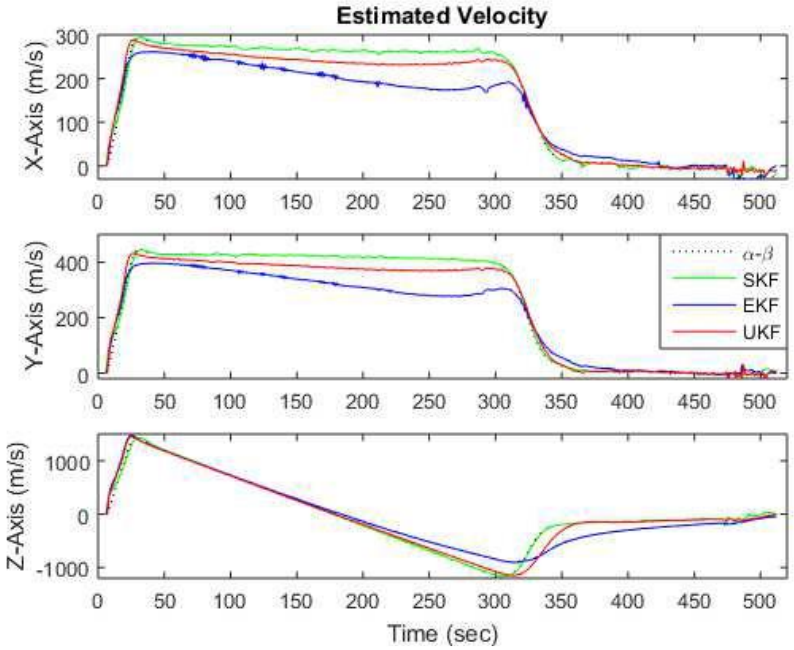

Source: MATLAB Implementation by Authors.

The results show that the UKF estimator exhibits the best performance in the powered ascent (ranging from 0-10 s for the 1-stg-rocket and 0-30 s for the 2-stg-rocket) and ballistic phases of flight.

Figures 6 to 9 show the estimated error and standard deviation on the three axes for the α-β, SKF, EKF, and UKF estimators.

Figure.6: (1-Stg Rocket) Error estimated by α-β, SKF, EKF, and UKF.

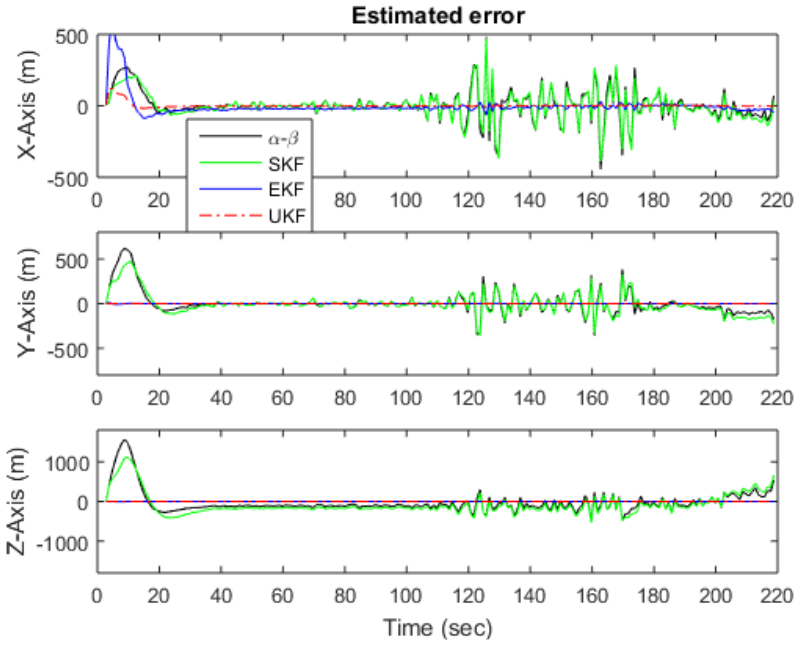

Source: MATLAB Implementation by Authors.

It can be observed that the estimation performances of the α-β and SKF are extremely similar in this application. Both have slow convergence and considerably large estimation error reaching 400 m, as seen on the X-axis in Fig. 6.

Figure.7. (2-Stg Rocket) Error estimated by α-β, SKF, EKF, and UKF.

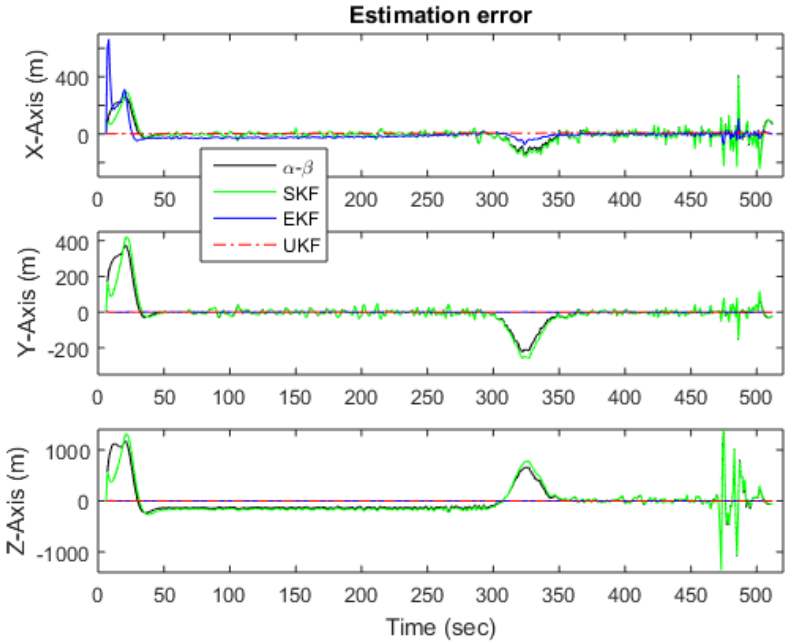

Source: MATLAB Implementation by Authors.

In addition, the EKF shows the largest estimation error during the powered ascent (ranging from 0-10 s for the 1-stg-rocket and 0-30 s for the 2-stg-rocket), only on the X-axis. At this stage, the EKF is more difficult to tune. For the remainder of the tracking, its performance is more accurate compared to the α-β filter and SKF and close to the UKF. This implies that the EKF converges to an acceptable estimate, but with instability and poor robustness. It is known that in certain situations, the problems of imprecision and divergence can occur as a consequence of the linearization of the nonlinear functions present in the algorithm.

The UKF shows smaller estimated error and standard deviation in the powered ascent (ranging from 0-10 s for the 1-stg-rocket and 0-30 s for the 2-stg-rocket, as shown in Figs. 6 to 9 of the flight. Thus, the UKF is more effective than the other estimators. The UKF exhibits the lowest estimated error and standard deviation in the parachute activation (ranging from 300--350 s for the 2-stg-rocket, as shown in Figs. 8 and 9. Hence, the UKF is more effective than the other estimators during changes in flight behavior.

Figure.8: (1-Stg Rocket) Standard deviation obtained by α-β, SKF, EKF, and UKF

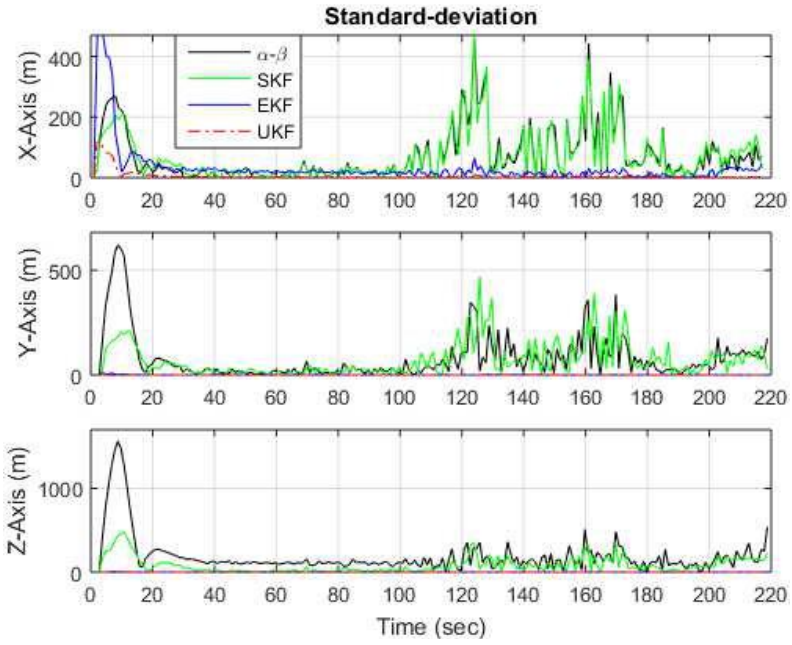

Source: MATLAB Implementation by Authors

Figure.9: (2-Stg Rocket) Standard deviation obtained by α-β, SKF, EKF, and UKF.

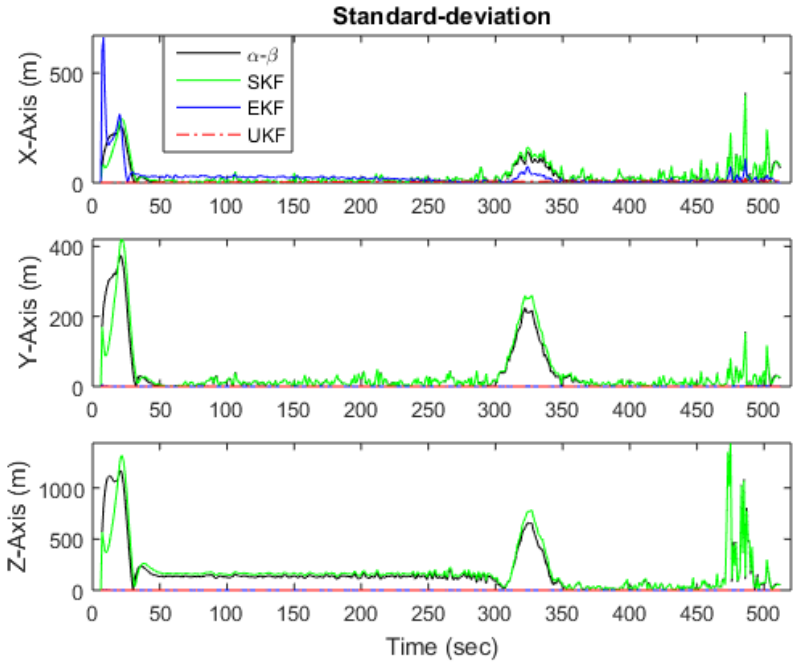

Source: MATLAB Implementation by Authors.

As discussed in Section 1, the contribution of this study is based on the results obtained with the UKF estimator, which proved to be the most optimistic, accurate, and stable in all flight phases. Tables 1 and 2 and Figs. 6 to 9 show that the UKF tracking algorithm reduces the measurement error of the radar sensor by 80% with respect to the EKF and 95%

with respect to the α-β and SKF. Table 3 shows the predicted IP (PIP) of the four tracking algorithms previously analyzed based on longitude (φ_k), latitude (λ_k), and impact time (t_k) coordinates for single-stage and two-stage rocket flight.

Table 3. PIP based on longitude (φ_k), latitude (λ_k), and flight time until impact (t_k).

	1-Stg Rocket			2-Stg Rocket		
	$\varphi_k\,(^o)$	$\lambda_k\,(^o)$	$t_k\,(s)$	$\varphi_k\,(^o)$	$\lambda_k\,(^o)$	$t_k\,(s)$
α-β	-43:50	-1:46	100:0	-43:00	-1:13	117:6
SKF	-43.51	-1.47	99.3	-43.01	-1.12	117.6
EKF	-43.51	-1.48	104.4	-43.00	-1.12	118.0
UKF	-43.52	-1.49	102.5	-43.01	-1.12	117.4

Source: Research data by Authors.

Figures 10 to 12 show the IPP and PIP of the four tracking algorithms for single-stage and two-stage rocket flight.

Figure.10: (1-Stg Rocket) IPP and PIP by α-β, SKF, EKF, and UKF estimators.

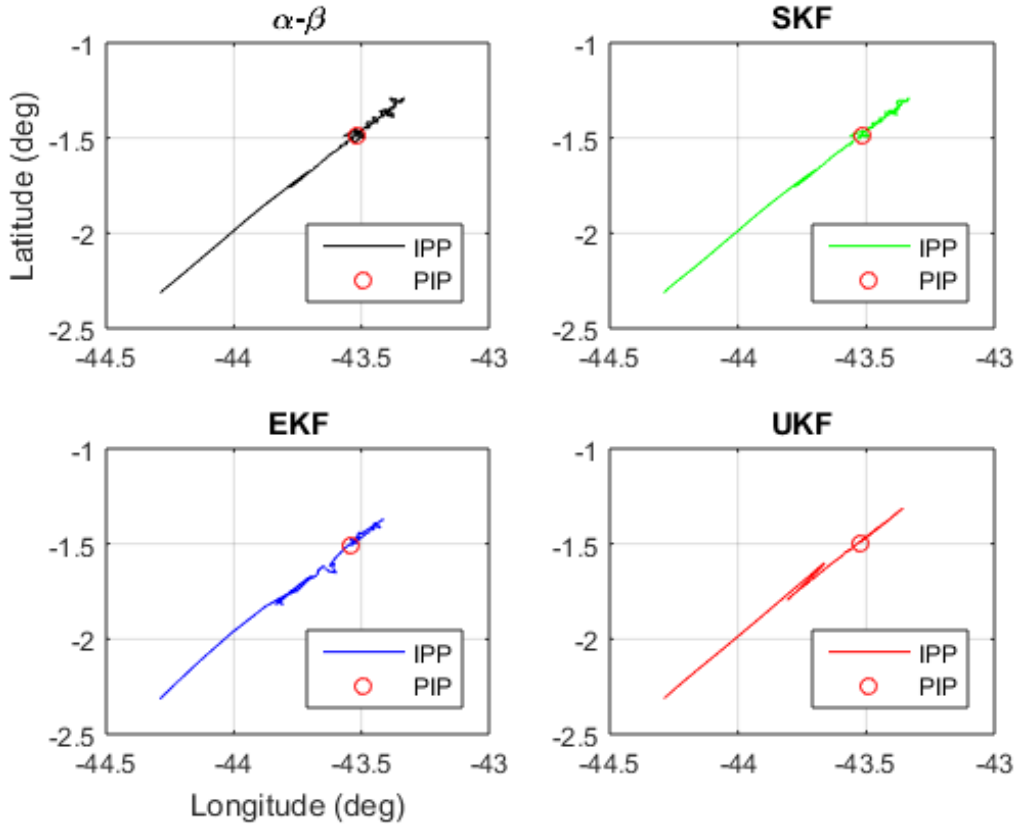

Source: MATLAB Implementation by Authors.

Figure.11: (1-Stg Rocket) IPP and PIP by α-β, SKF, EKF, and UKF (3D view)

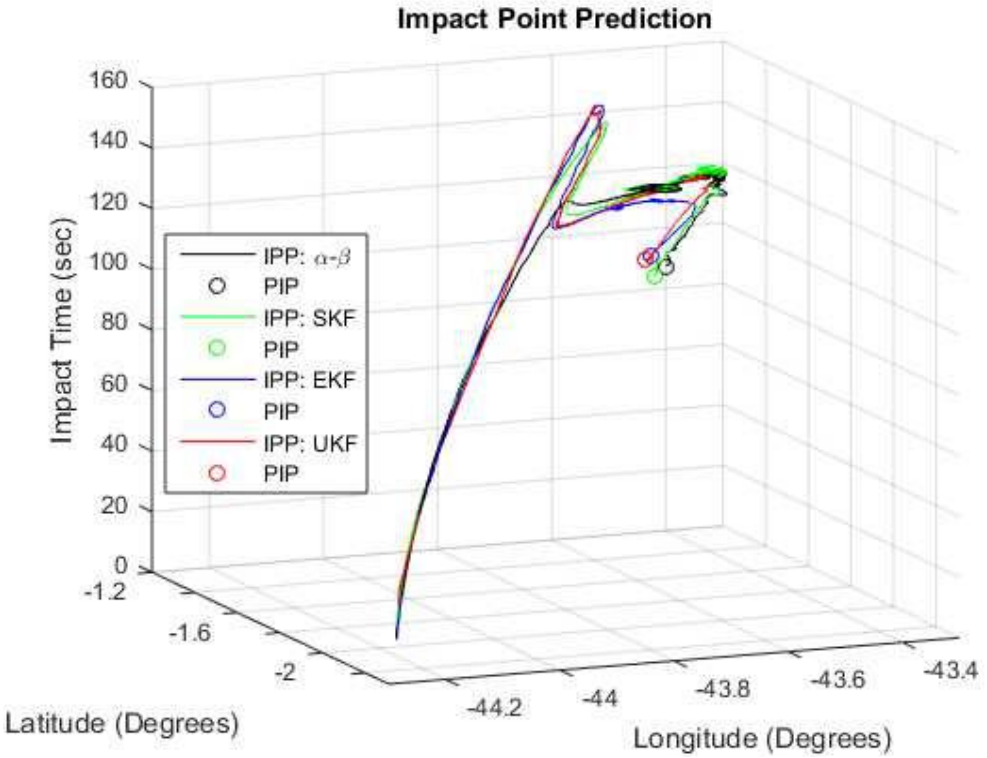

Source: MATLAB Implementation by Authors.

Figure.12: (2-Stg Rocket) IPP and PIP by α-β, SKF, EKF, and UKF (3D view)

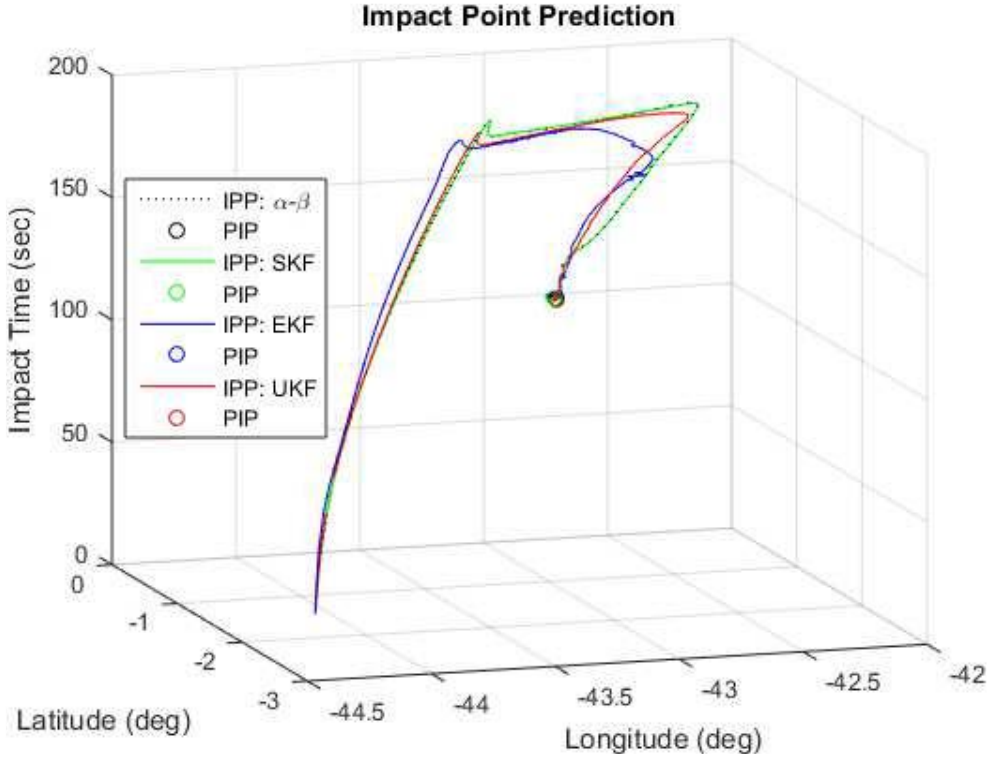

Source: MATLAB Implementation by Authors.

5. Conclusions

This study compared and evaluated the behavior of four different estimators used to improve rocket IPP, i.e., the α-β filter, SKF, EKF, and UKF. All four tracking algorithms, when designed and tuned appropriately, were able to track targets with a certain degree of accuracy. The advantages and disadvantages of all tracking algorithms were determined. The final results of this study used the actual data of rocket tracking measured using radar sensors. All four estimators appeared to be statistically efficient from the point of view of accuracy. The UKF outperformed all other tracking algorithms.

The estimation error and standard deviation of the α-β, SKF, EKF, and UKF estimators demonstrated that the best performance and, consequently, the main contribution of this work was obtained through the UKF tracking algorithm. This algorithm provided accurate performance and delineated under transient conditions, thereby contributing to the best IPP of suborbital rockets using a radar sensor.

References

Markgraf, M., Montenbruck, O., Turner, P., & Viertotak, M. (2003). Instantaneous impact point prediction for sounding rockets-perspectives and limitations. In European Rocket and Balloon Programmes and Related Research (Vol. 530, pp. 141-146).

Montenbruck, O., Markgraf, M., Jung, W., Bull, B., & Engler, W. (2002). GPS based prediction of the instantaneous impact point for sounding rockets. Aerospace Science and Technology, 6(4), 283-294.

Ramachandra, K. V. (2018). Kalman filtering techniques for radar tracking. CRC Press.

Simon, D. (2006). *Optimal state estimation: Kalman, H infinity, and nonlinear approaches*. John Wiley & Sons.

Kosuge, Y., Ito, M., Okada, T., & Mano, S. (2002). Steady-state errors of an α-β-γ filter for radar tracking. *Electronics and Communications in Japan (Part III: Fundamental Electronic Science)*, *85*(12), 65-79.

Ng, K. H., Yeong, C. F., Su, E. L. M., & Wong, L. X. (2012). Alpha beta gamma filter for cascaded PID motor position control. *Procedia Engineering*, *41*, 244-250.

Tenne, D., & Singh, T. (2002). Characterizing performance of alpha-beta-gamma filters. *IEEE Transactions on Aerospace and Electronic Systems*, *38*(3), 1072-1087.

Yadav, A., Naik, N., Ananthasayanam, M. R., Gaur, A., & Singh, Y. N. (2012). A constant gain Kalman filter approach to target tracking in wireless sensor networks. In *2012 IEEE 7th International Conference on Industrial and Information Systems (ICIIS)* (pp. 1-7). IEEE.

Abreu, J. A. P., Neto, J. V. F., & Oliveira, R. C. L. (2011). Ballistic rockets tracking: Kalman versus αβγ filters. In *2011 UkSim 13th International Conference on Computer Modelling and Simulation* (pp. 313-318). IEEE.

Chui, C. K., & Chen, G. (2008). Kalman filtering with real time applications. *Applied Optics*, *28*, 1841.

Kalman, R. E. (1960). A new approach to linear filtering and prediction problems. *Journal of basic Engineering*, *82*(1), 35-45.

Welch, G., & Bishop, G. (2006). *An introduction to the kalman filter. Chapel Hill, NC*. USA, Tech. Rep.

Garcia, A., Yamanaka, S. S. C., Barbosa, A. N., Bizarria, F. C. P., Jung, W., & Scheuerpflug, F. (2011). VSB-30 sounding rocket: history of flight performance. *Journal of Aerospace Technology and Management*, *3*(3), 325-330.

Einicke, G. A., & White, L. B. (1999). Robust extended Kalman filtering. *IEEE Transactions on Signal Processing*, *47*(9), 2596-2599.

Farina, A., Ristic, B., & Benvenuti, D. (2002). Tracking a ballistic target: comparison of several nonlinear filters. *IEEE Transactions on aerospace and electronic systems*, *38*(3), 854-867.

Biswas, S. K., Southwell, B., & Dempster, A. G. (2018). Performance analysis of Fast Unscented Kalman Filters for Attitude Determination. *IFAC-PapersOnLine*, *51*(1), 697-701.

Garcia, R. V., Pardal, P. C. P. M., Kuga, H. K., & Zanardi, M. C. (2019). Nonlinear filtering for sequential spacecraft attitude estimation with real data: Cubature Kalman Filter, Unscented Kalman Filter and Extended Kalman Filter. *Advances in Space Research*, *63*(2), 1038-1050.

Julier, S. J., & Uhlmann, J. K. (2004). Unscented filtering and nonlinear estimation. *Proceedings of the IEEE*, *92*(3), 401-422.

Scardua, L. A., & da Cruz, J. J. (2016). Particle-Based Tuning of the Unscented Kalman Filter. *Journal of Control, Automation and Electrical Systems*, *27*(1), 10-18.

Wan, E. A., & Van Der Merwe, R. (2000). The unscented Kalman filter for nonlinear estimation. In *Proceedings of the IEEE 2000 Adaptive Systems for Signal Processing, Communications, and Control Symposium (Cat. No. 00EX373)* (pp. 153-158). Ieee.

Garcia, R. V., Kuga, H. K., & Zanardi, M. C. F. (2016). Unscented Kalman filter for determination of spacecraft attitude using different attitude parameterizations and real data. *Journal of Aerospace Technology and Management*, *8*(1), 82-90.

Jung, J. K., & Hwang, D. H. (2013). The novel impact point prediction of a ballistic target with interacting multiple models. In *2013 13th International Conference on Control, Automation and Systems (ICCAS 2013)* (pp. 450-453). IEEE.

Wang, Z. Y., & Chang, S. J. (2013). Impact point prediction and analysis of lateral correction analysis of two-dimensional trajectory correction projectiles. *Defence Technology*, *9*(1), 48-52.

Bozic, S. M. Digital and Kalman Filtering: An Introduction to Discrete-time Filtering and Optimal Linear Estimation. 1983.

AminiOmam, M., Torkamani-Azar, F., & Ghorashi, S. A. (2017). Generalised Kalman-consensus filter. *IET Signal Processing*, *11*(5), 495-502.

Wu, C. M., Chang, C. K., & Chu, T. T. (2011). A new EP-based α–β–γ–δ filter for target tracking. *Mathematics and Computers in simulation*, *81*(9), 1785-1794.

Greco, M. S., Abramovich, Y., Ovarlez, J. P., Li, H., & Yang, X. (2015). Introduction to the issue on advanced signal processing techniques for radar applications. *IEEE Journal of Selected Topics in Signal Processing*, *9*(8), 1363-1365.

Gadsden, S. A., Dunne, D., Habibi, S. R., & Kirubarajan, T. (2009). Comparison of extended and unscented Kalman, particle, and smooth variable structure filters on a bearing-only target tracking problem. In *Signal and Data Processing of Small Targets 2009* (Vol. 7445, p. 74450B). International Society for Optics and Photonics.

Van Der Merwe, R. (2004). Sigma-point Kalman filters for probabilistic inference in dynamic state-space models (Doctoral dissertation, OGI School of Science & Engineering at OHSU).

Wan, E. (2006). Sigma-point filters: an overview with applications to integrated navigation and vision assisted control. In *2006 IEEE Nonlinear Statistical Signal Processing Workshop* (pp. 201-202). IEEE.

Porcentagem de contribuição de cada autor no manuscrito

José Alano Péres de Abreu – 50%

Roberto Célio Limão de Oliveira – 25%

João Viana da Fonseca Neto – 25%